1521-0111/103/4/221–229$35.00
MOLECULAR PHARMACOLOGY

dx.doi.org/10.1124/molpharm.122.000593
Mol Pharmacol 103:221–229, April 2023

Use-Dependent Relief of Inhibition of Nav1.8 Channels by A-887826

Sooyeon Jo,[1] Han-Xiong Bear Zhang,[1] and Bruce P. Bean

Department of Neurobiology, Harvard Medical School, Boston, Massachusetts

Received July 14, 2022; accepted December 9, 2022

ABSTRACT

Sodium channel inhibitors used as local anesthetics, antiarrhythmics, or antiepileptics typically have the property of use-dependent inhibition, whereby inhibition is enhanced by repetitive channel activation. For targeting pain, Nav1.8 channels are an attractive target because they are prominent in primary pain-sensing neurons, with little or no expression in most other kinds of neurons, and a number of Nav1.8-targeted compounds have been developed. We examined the characteristics of Nav1.8 inhibition by one of the most potent Nav1.8 inhibitors so far described, A-887826, and found that when studied with physiologic resting potentials and physiologic temperatures, inhibition had strong "reverse use dependence", whereby inhibition was relieved by repetitive short depolarizations. This effect was much stronger with A-887826 than with A-803467, another Nav1.8 inhibitor. The use-dependent relief from inhibition was seen in both human Nav1.8 channels studied in a cell line and in native Nav1.8 channels in mouse dorsal root ganglion (DRG) neurons. In native Nav1.8 channels, substantial relief of inhibition occurred during repetitive stimulation by action potential waveforms at 5 Hz, suggesting that the phenomenon is likely important under physiologic conditions.

SIGNIFICANCE STATEMENT

Nav1.8 sodium channels are expressed in primary pain-sensing neurons and are a prime current target for new drugs for pain. This work shows that one of the most potent Nav1.8 inhibitors, A-887826, has the unusual property that inhibition is relieved by repeated short depolarizations. This "reverse use dependence" may reduce inhibition during physiological firing and should be selected against in drug development.

Introduction

Voltage-dependent sodium channels underlie action potential firing of primary pain-sensing neurons ge(nociceptors), and inhibition of sodium channels is an attractive strategy for blocking pain signaling (Cummins et al., 2007; Dibb-Hajj et al., 2009; Bennett et al., 2019; Goodwin and McMahon, 2021). Many recent efforts to develop new drugs for pain have focused on developing selective inhibitors for Nav1.7 channels, which are expressed in peripheral neurons but have little expression in central neurons, and for Nav1.8 channels, which have even more restricted expression, including in C-fiber nociceptors (Han et al., 2016; Bennett et al., 2019; Goodwin and McMahon, 2021; Jayakar et al., 2021). A number of compounds with selectivity for inhibiting Nav1.8 channels over other sodium channel types have been reported (Payne et al., 2015: Brown et al., 2019; Urru et al., 2020; reviewed by Obeng et al., 2021; Yekkirala et al., 2017; Han et al., 2016), and at least one has advanced into human clinical trials (Hijma et al., 2021).

So far, the most potent and selective Nav1.8 inhibitors that have been described are A-803467, with reported >100-fold selectivity for inhibition of Nav1.8 channels over Nav1.2, Nav1.3, Nav1.5, and Nav1.7 channels (Jarvis et al., 2007) and A-887826, with higher potency for Nav1.8 but somewhat less selectivity over other sodium channels (Zhang et al., 2010). Both A-803467 and A-887826 reduce inflammatory and neuropathic pain in rodent pain models (Jarvis et al., 2007; Joshi et al., 2009; Zhang et al., 2010; Chen et al., 2014; Rahman and Dickenson, 2015; Laux-Biehlmann et al., 2016).

An unusual feature of A-803467 inhibition of Nav1.8 channels was seen when studying inhibition during trains of depolarizing pulses (Browne et al., 2009a, b). Unlike the typical use-dependent enhancement of inhibition seen with classic small-molecule sodium channel inhibitors like lidocaine, phenytoin, and carbamazepine (Cummins and Rush, 2007), A-803467 inhibition of the human Nav1.8 channel actually showed a modest reduction of inhibition when 10-millisecond steps to 0 mV were applied at 10 Hz from a holding potential of −120 mV (Browne et al., 2009a, b).

Here, we have studied the state-dependent interaction with Nav1.8 channels of the more potent inhibitor A-887826. We find a much more prominent use-dependent relief of inhibition compared with A-803467. This effect was seen at physiologic temperatures and membrane potentials with both cloned human Nav1.8 channels studied in a cell line and in native Nav1.8 channels in mouse dorsal root ganglion (DRG) neurons, where it was present during repetitive stimulation by action potential waveforms at 5 Hz, suggesting importance

This work was supported by National Institutes of Health National Institute of Neurological Disorders and Stroke [Grant R01-NS036855] (to B.P.B.), [Grant R01-NS110860] (to B.P.B.), and [Grant R35-NS127216] (to B.P.B.).
No author has an actual or perceived conflict of interest with the contents of this article.
[1]S.J. and H.-X.B.Z. contributed equally to this work.
dx.doi.org/10.1124/molpharm.122.000593.

ABBREVIATIONS: hNav1.8 channel, human Nav1.8 sodium channel.

under physiologic conditions. Analysis of the dependence of the effect on pulse length suggests that it arises from reduced affinity of A-887826 binding to inactivated states of the channel rather than open states of the channel.

Materials and Methods

Pharmacology A-887826 and A-803467 were obtained from Sigma-Aldrich, prepared as a stock solution of 10 mM in DMSO (Sigma-Aldrich), and diluted as final concentrations of 30–1000 nM in recording solution.

Electrophysiology of Human Nav1.8 Cell Line. A cell line stably expressing human Nav1.8 α- and β3-subunits in Chinese hamster ovary (CHO-K1) cells was purchased from B'SYS GmbH and grown in Ham's F-12 medium (Corning) containing 10% FBS, penicillin/streptomycin (Sigma), and 3.5 μg/ml puromycin (Sigma) and 350 μg/ml hygromycin (Sigma) under 5% CO_2 at 37°C. For electrophysiological recordings, cells were replated on coverslips for 1–6 hours before recording. Whole-cell recordings were obtained using patch pipettes with resistances of 1.8–2.2 MΩ when filled with the internal solution, consisting of 61 mM CsF, 61 mM CsCl, 9 mM NaCl, 1.8 mM $MgCl_2$, 9 mM EGTA, 14 mM creatine phosphate (Tris salt), 4 mM MgATP, 0.3 mM GTP (Tris salt), and 9 mM HEPES, pH adjusted to 7.2 with CsOH. The shank of the electrode was wrapped with Parafilm to reduce capacitance and allow optimal series resistance compensation without oscillation. Seals were obtained and the whole-cell configuration established with cells in Tyrode's solution consisting of 155 mM NaCl, 3.5 mM KCl, 1.5 mM $CaCl_2$, 1 mM $MgCl_2$, 10 mM HEPES, and 10 mM glucose, pH adjusted to 7.4 with NaOH. After establishing whole-cell recording, cells were lifted off the bottom of the recording chamber and placed in front of an array of quartz flow pipes (250-μm internal diameter, 350-μm external; Polymicro Technologies) attached with styrene butadiene glue (Amazing Goop, Eclectic Products) to an aluminum rod (1 × 1 cm) whose temperature was controlled to 38°C by resistive heating elements and a feedback-controlled temperature controller (TC-344B; Warner Instruments). With the end of the rod and the flow pipes (extending 1 mm from the end of the rod) lowered just below the surface of the bulk chamber solution, the solution exiting from the flow pipes is maintained at 37°C (Carter and Bean, 2009). Recordings were made using a base external solution of Tyrode's solution with added 10 mM TEACl. Solution changes were made (in <1 second) by moving the cell between adjacent pipes. Typically, sodium currents increased with time after the start of whole-cell recording, perhaps reflecting removal of long-term inactivation from the relatively depolarized resting potential typical of CHO cells. Recording of control currents was started after this run-up reached a near steady state, typically about 10 minutes after establishing whole-cell recording.

The amplifier was tuned for partial compensation of series resistance (typically 70%–80% of a total series resistance of 4–10 MΩ), and tuning was periodically readjusted during the experiment. Currents were recorded at 37°C with an Axon Instruments Multiclamp 700B Amplifier (Molecular Devices) and filtered at 5 kHz with a low-pass Bessel filter. Currents were digitized using a Digidata 1322A data acquisition interface controlled by pClamp9.2 software (Axon Instruments) and analyzed using programs written in Igor Pro 6 (Wavemetrics, Lake Oswego, OR), using DataAccess (Bruxton Software) to read pClamp files into Igor Pro.

Currents were corrected for linear capacitative and leak currents, which were determined using 5-mV hyperpolarizations delivered from the resting potential and then appropriately scaled and subtracted. The correction for capacitative current is imperfect, as evident by remaining transients after linear correction, probably because of nonlinearities in the recorded current resulting from head-stage amplifier saturation for large steps. These remaining transients sometimes overlapped with the initial rising phase of the sodium current but were brief enough that they did not interfere with measurements of peak current (Fig. 2). The correction of leak currents assuming linearity was sometimes also imperfect as evidenced by corrected steady-state currents that were slightly outward in some cells after sodium current had been greatly reduced by A-887826. The calculations based on measurements of persistent current during the 500-millisecond steps in the presence of A-887826 in Fig. 4 were therefore confined to cells in which the minimum persistent inward current during the step was at least 40 pA.

We calculated the error remaining from incomplete compensation for series resistance in each cell by multiplying the series resistance that remained uncompensated by the peak current amplitude. The mean error was 3.5 mV ± 2.7 mV (mean ± standard deviation, n = 120). The error in all cells was <10 mV. Because all errors >6 mV were for currents in control conditions for protocols using test pulses to +20 mV, near the peak of the current-voltage relation (Fig. 2) where a deviation of voltage by 10 mV would have very little effect on peak current magnitude, we did not exclude data from these cells.

Data are given as mean ± S.E.M.

Electrophysiology of Mouse DRG Neurons. Acutely dissociated DRG neurons were prepared as previously described (Liu et al., 2017; Zhang and Bean, 2021). Experiments were carried out in accordance with the Guide for the Care and Use of Laboratory Animals as adopted and promulgated by the US National Institutes of Health and were approved by the Harvard Medical School Institutional Animal Care and Use Committee (Protocol 02538). Briefly, DRG neurons were removed from Swiss Webster mice (P23-P37) with their roots trimmed and treated for 20 minutes at 37°C with 20 U/ml papain (Worthington Biochemical, Lakewood, NJ) in a calcium- and magnesium-free Hank's buffer containing 137 mM NaCl, 5.36 mM KCl, 0.33 mM Na_2HP4, 0.44 mM KH_2PO4, 5 mM HEPES, 5.55 mM glucose, and 0.001% phenol red, pH 7.40 adjusted with NaOH; 300–310 mOsm. Ganglia were then treated for 20 minutes at 37°C with 3 mg/ml collagenase (type I; Roche Diagnostics, Indianapolis, IN) and 4 mg/ml dispase II (Roche Diagnostics) in calcium- and magnesium-free Hank's buffer. Cells were dispersed by trituration with a fire-polished glass Pasteur pipette in a solution composed of two media combined in a 1:1 ratio: Leibovitz's L-15 medium (Invitrogen, Grand Island, NY) supplemented with 5 mM HEPES and DMEM/F12 medium (Invitrogen) supplemented with 10% Heat-Inactivated Fetal Bovine Serum (ThermoFisher) and 130 ng/ml nerve growth factor (Invitrogen). Cells were then incubated at 37°C (95% O_2, 5% CO_2) for 2 hours, after which Neurobasal medium (Invitrogen) containing 1X B-27 supplement (Invitrogen), penicillin and streptomycin (Sigma, St. Louis, MO), and 200 ng/ml nerve growth factor was added to the petri dish. Cells were stored at 4°C and used within 48 hours.

Whole-cell voltage-clamp recordings were made from DRG neurons using an Axon Instruments Multiclamp 700B Amplifier (Molecular Devices). Electrodes had resistances of 3–6 MΩ, with tips wrapped by Parafilm. The internal solution was 140 mM CsCl, 13.5 mM NaCl, 1.8 mM $MgCl_2$, 0.09 mM EGTA, 9 mM HEPES, 14 mM creatine phosphate (Tris salt), 4 mM MgATP, and 0.3 mM Tris-GTP, pH adjusted to 7.2 with CsOH. Seals were formed in Tyrode's solution (155 mM NaCl, 3.5 mM KCl, 1.5 mM $CaCl_2$, 1 mM $MgCl_2$, 10 mM HEPES, and 10 mM glucose, pH 7.4 adjusted with NaOH). After establishing whole-cell recording, cell capacitance was nulled and series resistance was partially (70%–80%) compensated. Cells were lifted and placed in front of temperature-controlled quartz flow pipes. Recordings were made of tetrodotoxin (TTX)-resistant sodium current at 37°C using an external solution designed to isolate TTX-resistant sodium currents by adding 30 μM $CdCl_2$ to inhibit calcium currents, 10 mM TEACl to inhibit potassium currents, and 300 nM TTX to inhibit TTX-sensitive sodium currents. Procedures for recording and analysis followed those for the hNav1.8 cell line experiments. For action potential clamp currents, leak and residual capacitative currents were determined using signal-averaged hyperpolarizations from −70 to −72 mV, and leak and residual capacitative currents were then subtracted in a point-by-point manner. In some cases with nearly complete inhibition of sodium current, there was a small outward current evoked by the

action potential waveform, probably reflecting incomplete inhibition of potassium channels. In these cases, peak sodium current during the rising phase of the action potential was measured relative to a baseline of this outward current, as illustrated in Fig. 9B. Experiments were done using small-diameter DRG neurons (8.8 ± 0.34 pF), all of which (27 of 27 neurons tested) expressed sodium currents resistant to 300 nM TTX, with the signature slow inactivation and relatively depolarized steady-state inactivation curves compared with TTX-sensitive sodium currents (Roy and Narahashi, 1992; Rush et al., 1998; Blair and Bean, 2002). Under our recording conditions, the voltage dependence and kinetics of the TTX-R sodium current suggest that it is almost entirely from Nav1.8 channels, with little or no contribution from Nav1.9 (Cummins et al., 1999; Blair and Bean, 2003; Bosmans et al., 2011).

We calculated the error remaining from incomplete compensation for series resistance in each cell. All errors were less than 6 mV (mean 2.3 mV ± 1.7 mV standard deviation, $n = 20$), and since all errors >3.5 mV was in control solutions in cells in which the measurement of test pulse current was made at 0 mV or +20 mV, near the peak of current-voltage relation, such errors will have minimal effect on the calculated effect of drug.

Data are given as mean ± S.E.M.

Results

Use-Dependent Relief of Inhibition by A-887826. Fig. 1A shows the inhibition of sodium current by A-887826 in cells stably expressing human Nav1.8 α subunits together with β3 subunits. When assayed at 37°C using step depolarizations applied from a steady holding voltage of −70 mV, typical of normal neuronal resting potentials, 30 nM A-887826 inhibited peak sodium current to 41 ± 4% of control (mean ± SEM, $n = 15$) after 1 minute of application. Inhibition by A-887826 was substantially more potent than by A-803467 using the same protocol, where 100 nM A-803467 was required to produce ~50% inhibition (reducing current to 52 ± 5% of control, $n = 6$).

The hNav1.8 current inactivated incompletely during 20-millisecond depolarizations. Both A-887826 and A-803467 inhibited both peak transient current and the persistent component of current that remained at the end of 20-millisecond steps. The two components of current were inhibited with a similar time course by both A-887826 and A-803467 (Fig. 1, B and D). For both compounds, persistent current was apparently inhibited to a slightly greater degree than the peak transient current, but the difference was small (Fig. 1, B and D). Accurate quantification of the persistent current after it has been reduced by drug could be influenced by imperfect correction for leak current, which is assumed to be linear with voltage but may not always be. Because of this, it is difficult to be sure that the small apparent difference in reduction of the persistent versus transient current is real.

Fig. 2 shows the current-voltage relationship for hNav1.8 current before and after application of 30 nM A-887826. Currents were inhibited over the full range of voltage steps. Outward as well as inward currents were inhibited, and there was no change in the reversal potential for the current, near +70 mV. The lack of change in the current-voltage relationship by A-887826 is consistent with the lack of change in activation curves seen previously for TTX-resistant sodium current in rat DRG neurons (Zhang et al., 2010).

A striking feature of inhibition of Nav1.8 current by A-887826 is that it was relieved by repetitive stimulation at moderate frequencies. Fig. 3A shows an example, where after 30 nM A-887826 inhibited current to ~10% of initial control, a train of 100 5-millisecond depolarizations to +20 mV delivered at 5 Hz produced a dramatic enhancement of current, increasing peak current ~fivefold. In collected results with this protocol, currents in 30 nM A-887826 were 0.27 ± 0.03 of control values before the train and 0.55 ± 0.02 after the train ($n = 10$). As reported previously, there was also use-dependent relief of inhibition by A-803467 (Browne et al.,

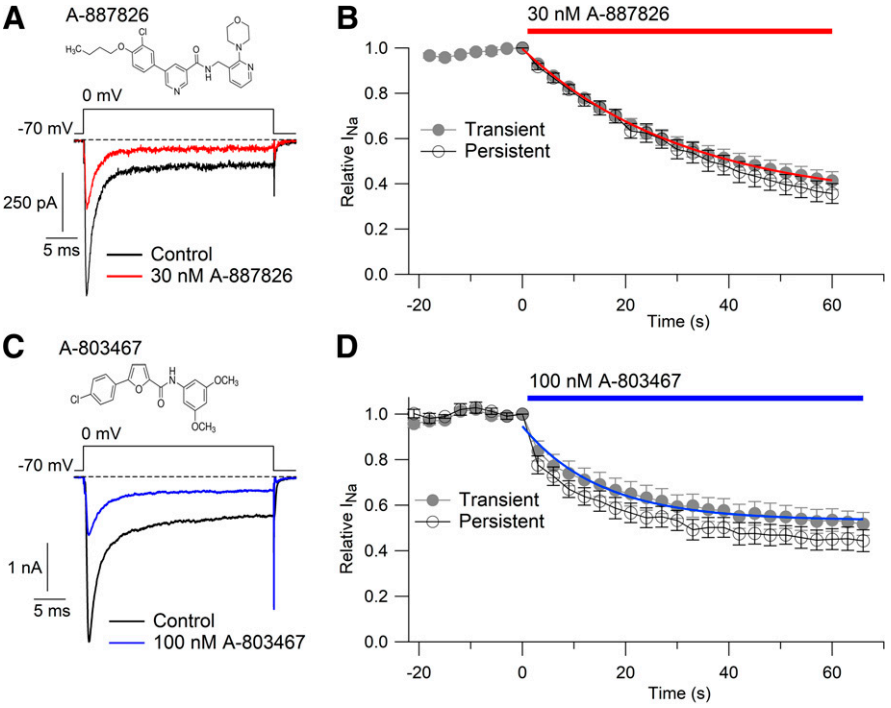

Fig. 1. Slow but effective inhibition of human Nav1.8 channels by 30 nM A-887826. (A) hNav1.8 current evoked by a 30-millisecond depolarization from −70 mV to 0 mV before and after application of 30 nM A-887826. (B) Time course of inhibition by 30 nM A-887826. Current was evoked by 30-millisecond test pulses from −70 mV to 0 mV delivered every 3 seconds. Collected results, mean ± S.E.M., $n = 15$. Filled circles: peak transient current. Open circles: persistent current at the end of the test pulse. Solid red line: fit to exponential function with time constant 32 seconds and asymptote 0.31. (C) Effect of 100 nM A-803467 tested with the same voltage protocol. (D) Time course of inhibition by 100 nM A-803467. Collected results, mean ± S.E.M., $n = 6$. Filled circles: peak transient current. Open circles: persistent current at the end of the test pulse. Solid blue line: exponential function fit to time course of peak transient current with time constant 15 second and asymptote 0.53.

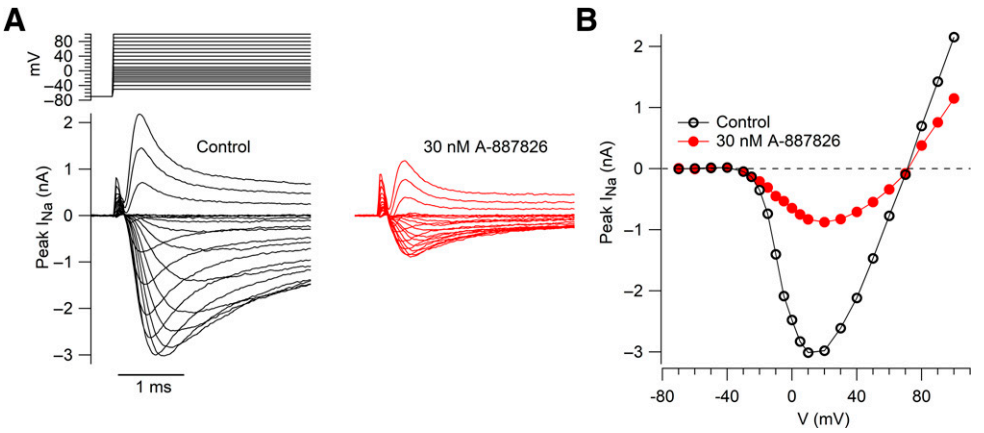

Fig. 2. Peak current versus voltage relationship for hNav1.8 channels before and after inhibition by 30 nM A-887826. (A) Currents evoked by 3-millisecond depolarizations from a holding potential of −70 mV to test voltages ranging from −50 to +110 mV before (left) and after (right) application of 30 nM A-887826. (B) Peak current as a function of test voltage before (open black circles) and after (filled red circles) application of 30 nM A-887826.

2009a, b), but it was far less dramatic; in 100 nM A-803467, current increased from 0.55 ± 0.04 of control values before the train to 0.58 ± 0.05 of control after the train.

Dependence on Pulse Duration. Fig. 4 shows an experiment examining how the degree of use-dependent relief of inhibition depends on pulse duration. This experiment used trains of depolarizations to +20 mV with varying pulse durations, delivered at 2 Hz in each case, but with different numbers of pulses in the train such that the total time at +20 mV during the train was 500 milliseconds. This experiment was designed to test whether reversal of inhibition involves drug unbinding from the open state of the channel or the inactivated state. With short steps, channels are mainly in the open state, whereas with longer steps, channels are first in the open state but then mainly in the inactivated state (Fig. 4B). The experiment showed that there was strikingly more reversal of inhibition with longer steps. Thus, 500 1-millisecond steps produced a fractional relief of inhibition (current after the train relative to that in the control before application of A-887826) to an average of 0.18 ± 0.05 (n = 7), whereas 25 20-millisecond steps produced a relief of inhibition to 0.41 ± 0.03 (n = 9). Comparing the degree of relief of inhibition to the total time channels spend in the open state or inactivated state during the train of pulses showed that the degree of reversal inhibition is much better correlated with time spent in the inactivated state than in the open state (Fig. 4C). Also, the time constant of relief of inhibition was much faster with longer duration pulses during the train (Fig. 4D), consistent with drug unbinding throughout the pulse and not just in the first msec or so when channels are maximally open. Overall, the simplest interpretation of the results is that drug unbinds mainly from channels in the inactivated state. However, although channels are mostly in the inactivated state during the longer steps, there is also a fraction of channels still open, producing the component of persistent current. It is possible that the relief of inhibition could also involve unbinding from channels open during the persistent current.

Relief of Inhibition During Long Depolarizing Steps. With maintained depolarizations, Nav1.8 channels enter into a slow inactivated state (Rush et al., 1998; Blair and Bean, 2003; Tripathi et al., 2006; Choi et al., 2007; Zhang and Bean, 2021). To explore whether relief of A-887826 inhibition might occur

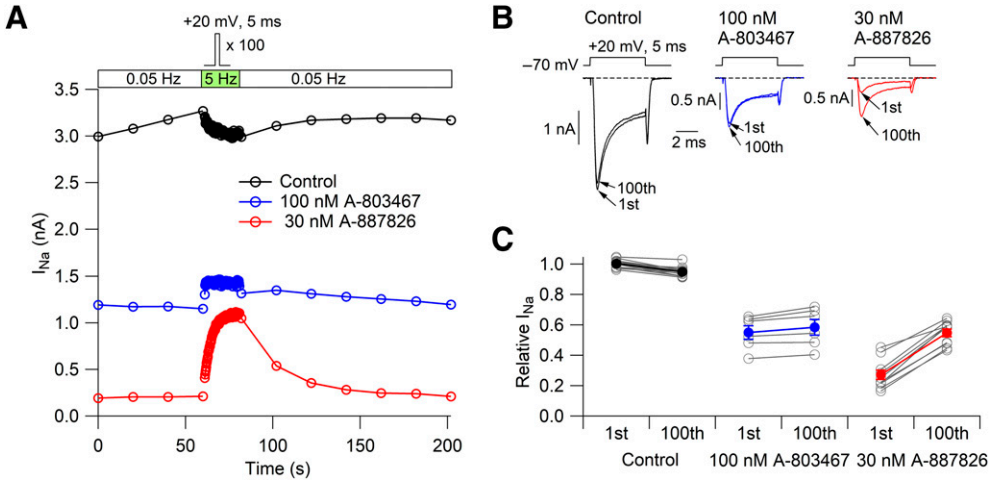

Fig. 3. Use-dependent relief of A-887826 inhibition of hNav1.8 channels. (A) Effect of a series of 5-millisecond steps to +20 mV delivered at 5 Hz on peak current in control (black), 30 nM A-887826 (red), and 100 nM A-803467 (blue). (B) The current evoked by the first and 100th steps in the series in each of the conditions. (C) Collected results with this protocol. Current was normalized to the current in control solution (during slow stimulation) before application of A-887826 or A-803467. Control: decrease from 1.003 ± 0.0007 on first pulse at 5 Hz to 0.949 ± 0.009 on 100th pulse, n = 13; P = 0.0024, two-tailed Wilcoxon signed-rank test. A-803467: increase from 0.55 ± 0.04 to 0.58 ± 0.05, n = 6; P = 0.13, two-tailed paired t test (sample size too small for Wilcoxon test). A-887826: increase from 0.27 ± 0.03 to 0.55 ± 0.02, n = 10; P = 0.0054, two-tailed Wilcoxon signed-rank test.

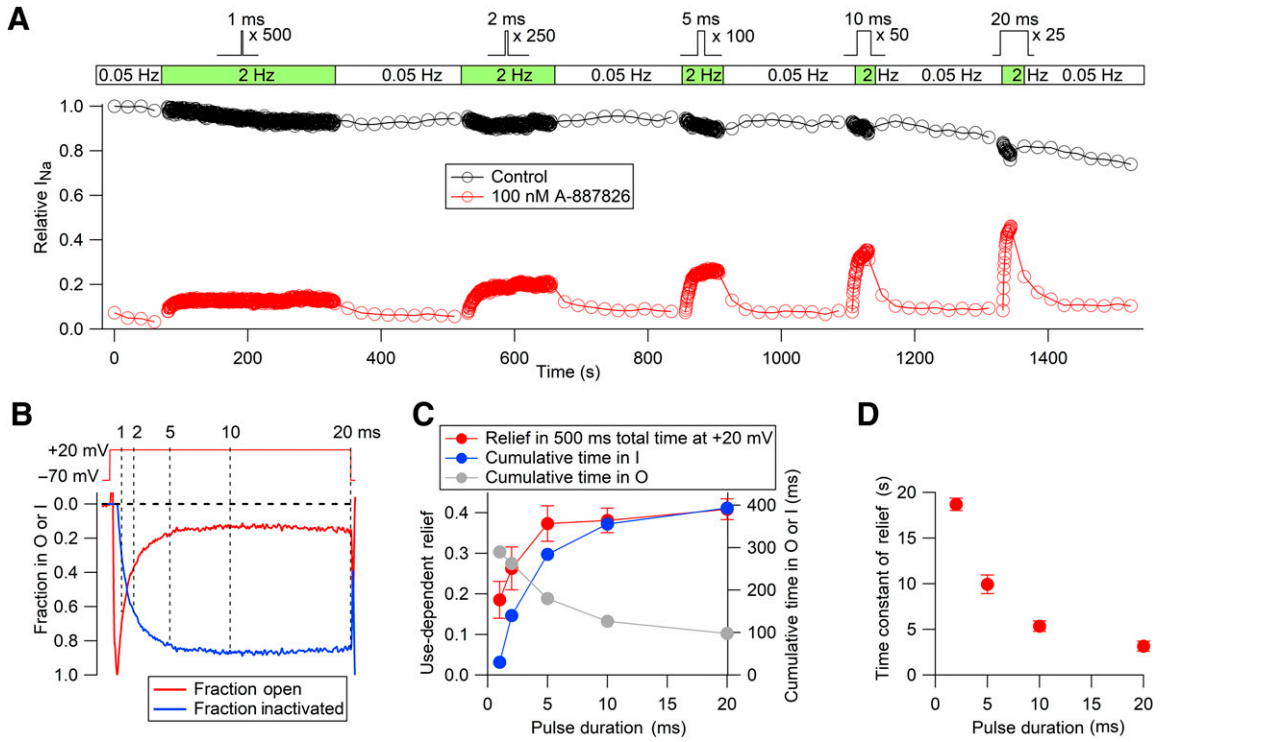

Fig. 4. Effect of pulse length on use-dependent relief of inhibition of hNav1.8 channels by A-887826. (A) Relative peak current evoked by steps to +20 mV in control (black) or 100 nM A-887826 (red) during trains of steps of different durations to relieve inhibition. Current was normalized to the current in control solution (during slow stimulation) before application of A-887826. (B) Time course of occupancy of the open state (red) and inactivated state (blue) during a 20-millisecond step to +20 mV. Recorded in 100 nM A-887826. Fraction of channels open is calculated as proportional to peak recorded current (red, 137 pA peak inward current), and fraction of inactivated channels is calculated as 1-fraction open. Vertical dashed lines illustrate occupancy during pulses of various durations. (C) Comparison of degree of recovery for trains of each pulse duration (each with a total time at +20 mV of 500 milliseconds) with total time in the open or inactivated state (calculated by multiplying integrated time in the state during a single pulse by the number of pulses in the train). Red: collected results for relief of inhibition (current after the train normalized to the current evoked before application of A-887826; n = 7, 7, 8, 9, 9 for determinations with pulses of 1, 2, 5, 10, and 20 millisecond). Gray: cumulative time in the open state during 500 millisecond total time at +20 mV. Blue: cumulative time in the inactivated state. (D) Collected results for time-constant of recovery of currents during trains with different pulse durations.

from slow inactivated states as well as the fast inactivated states that would predominate with short depolarizations, we compared relief of inhibition produced by a single long 500-millisecond depolarizing step, which would place a substantial fraction of channels in slow inactivated states, with repeated short (20-millisecond) depolarizing steps of the same total duration (Fig. 5). A single 500-millisecond step to +20 mV produced very similar relief of inhibition by 30 nM A-887826 (from 0.22 ± 0.04 before the prepulse to 0.51 ± 0.02 afterward, normalized to initial control current before the prepulse) as a sequence of 20-millisecond depolarizations given at 2 Hz for the same 500-millisecond total duration (from 0.26 ± 0.04 to 0.54 ± 0.03; n = 6; protocols in the same cells). During 500-millisecond steps to +20 mV, relief of inhibition was also evident as a gradual growth of the persistent component of current during the step once the initial phase of inactivation was over, after the first 50 milliseconds or so (Fig. 5C). When normalized to the minimum inward current during the 500-millisecond step in control, reached at the end of the step (position c in Fig. 5C), the current in the presence of A-887826 increased from 0.32 ± 0.05 at its minimum, reached at 50–100 milliseconds during the step, to 0.50 ± 0.04 at the end of the step (n = 6).

To help interpret the relief of inhibition during 500-millisecond steps, we examined the inhibition by A-887826 using 500-millisecond steps to a range of voltages between −100 mV to +40 mV, either followed immediately by a test step to +20 mV (Fig. 6A) or with a 10-millisecond return to −100 mV before the test step (Fig. 6B). In separate experiments, we determined that the 10-millisecond return to −100 mV allows complete recovery from fast inactivation in control, so the protocol assays the fraction of channels that enter into slow inactivated states. These protocols yielded striking results: with both protocols, the inhibition by A-887826 was dramatically relieved in a voltage-dependent manner for 500-millisecond depolarizations progressing from −10 mV to +40 mV. Because the fraction of channels in slow inactivated states does not change much in the region between −10 and +40 mV, the results are not easily interpreted as reflecting more relief of inhibition as more channels enter a slow inactivated state. Similarly, the fraction of channels in the fast inactivated state (assayed by the fraction of channels that recover availability during the 10-millisecond return to −100 mV in the protocol in Fig. 6B) also does not change much between −10 mV and +40 mV, so the steep voltage dependence of relief of inhibition in this voltage range is not obviously correlated with the occupancy of fast inactivated states.

Overall, the results seem consistent with the idea that A-887826 binding can be relieved when channels are in either fast inactivated or slow inactivated states.

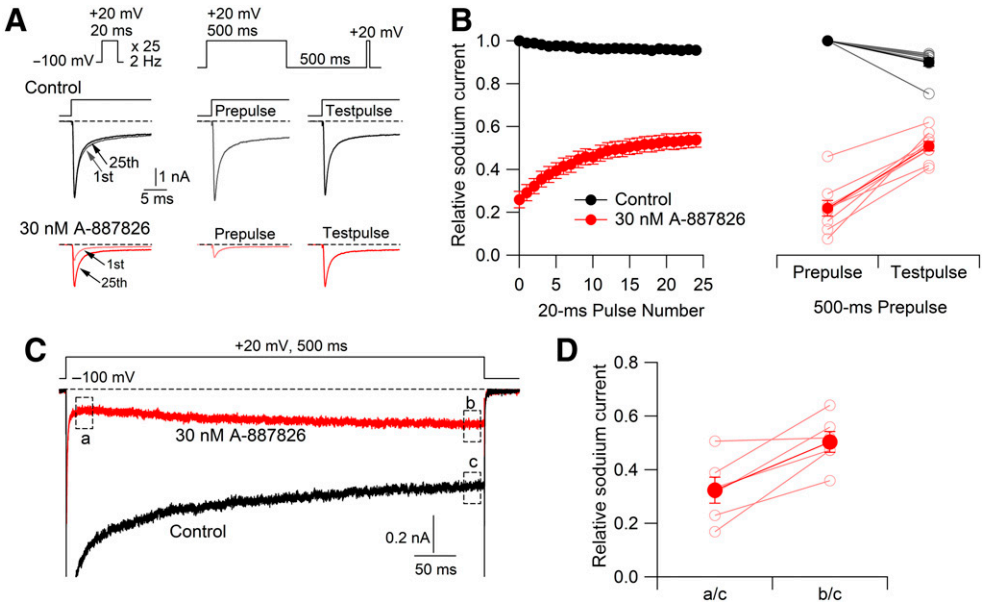

Fig. 5. Reversal of A-887826 inhibition of hNav1.8 channels by a single 500-millisecond depolarization compared with repeated 20-millisecond depolarizations of the same total duration. (A) Left: currents evoked by 20-millisecond steps to +20 mV delivered every 500 milliseconds for 12 seconds (25 steps). Right: currents evoked at the start of a 500-millisecond prepulse to +20 mV and by a test pulse delivered 500 milliseconds after the end of the prepulse. Top: currents in control. Bottom: currents after application of 30 nM A-887826. Currents from the same cell are shown for all protocols. (B) Collected results for this protocol in nine cells, showing mean ± S.E.M. for relative current (normalized to current in control for the first 20-millisecond pulse or the start of the 500-millisecond prepulse in control). (C) Illustration of apparent reversal of inhibition during a single 500-millisecond step to +20 mV. (D) Collected results for apparent reversal of inhibition during 500-millisecond step to +20 mV in six cells. To quantify the effect, the smallest current during the step with A-887826 was normalized to the smallest current in control (reached at the end of the step) and compared with the current at the end of the step in A-887826, normalized in the same way. Mean ± S.E.M., $n = 6$.

Without further experiments and detailed modeling, it seems difficult to determine if there is any difference in drug unbinding from fast inactivated versus slow inactivated states, especially because the steep voltage-dependence of relief in the range from −10 mV to +40 mV does not obviously correspond to a major difference in the relative occupancy of the two states. It is also possible that the relief of inhibition involves drug unbinding from open states during the persistent current occurring during moderately long depolarizations. The occupancy of persistent open states does not obviously change dramatically in the range from −10 mV to +40 mV, but it is difficult to quantify the persistent current for larger depolarizations where driving force decreases and the persistent current gets small (especially after inhibition by A-887826) since accurate quantification depends on the accuracy of correction of leak current, which is likely imperfect.

Use-Dependent Relief of Inhibition in Native Mouse Nav1.8 Currents. Gating behavior of channels and state-dependent interaction with inhibitors can be affected by accessory subunits, for which full knowledge is lacking for most native channels. We were therefore interested in examining the characteristics of inhibition by A-887826 for native Nav1.8 channels and performed a series of experiments on TTX-resistant sodium channels in small-diameter acutely-dissociated mouse DRG neurons. A-887826 effectively inhibited native mouse Nav1.8 currents (Fig. 7). Interestingly, however, the sensitivity of native mouse channels to A-887826 was about 10-fold lower than for human Nav1.8/beta3 in CHO cells, with a half-blocking concentration of about 300 nM (Fig. 7). The inhibition of native mouse TTX-resistant sodium current by 1 μM A-887826 (80 ± 2% inhibition, $n = 5$) was similar to the inhibition of hNav1.8 channels by 100 nM A-887826 (86 ± 2% inhibition, $n = 17$).

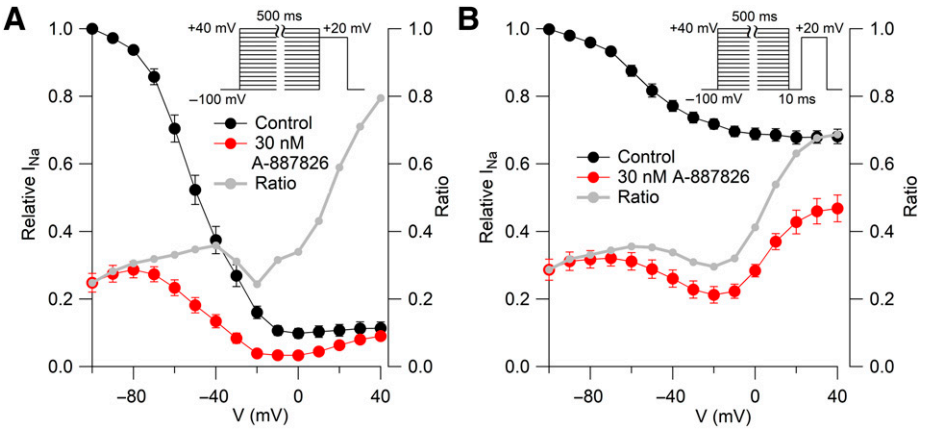

Fig. 6. Voltage dependence of A-887826 inhibition of hNav1.8 channels with 500-millisecond depolarizations. (A) Relative peak current evoked by steps to +20 mV in control (black) or 30 nM A-887826 (red) after 500-millisecond depolarizations to voltages between −100 mV and +40 mV. Current was normalized to the current in control solution evoked from the steady holding voltage of −100 mV. Mean ± S.E.M., $n = 9$. Gray: ratio of mean values in A-887826 divided by mean values in control. (B) Relative peak current evoked by steps to +20 mV in control (black) or 30 nM A-887826 (red) after 500-millisecond depolarizations to voltages between −100 mV and +40 mV followed by a 10-millisecond return to −100 mV, which in control allows recovery from fast inactivation. Mean ± S.E.M., $n = 9$. Gray: ratio of mean values in A-887826 divided by mean values in control.

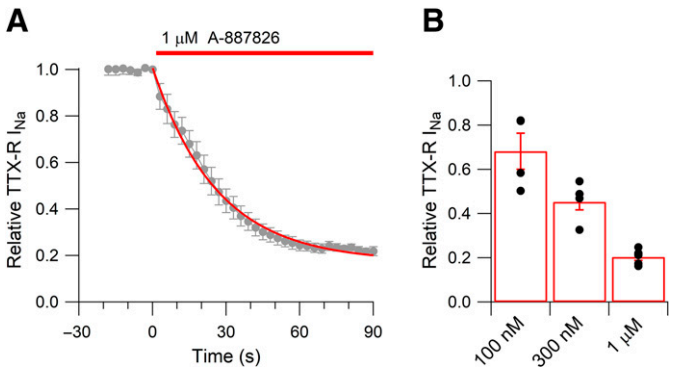

Fig. 7. Dose-dependent inhibition of TTX-R Na channels in mouse nociceptive neurons by A-887826. (A) Time course of inhibition by 1 μM A-887826. Current was evoked by 30-millisecond voltage steps from −70 mV to 0 mV delivered every 3 seconds. Mean ± S.E.M. for five cells for times to 69 seconds and for four cells from times from 72 to 90 seconds. Solid red line: exponential fit, with time constant 26 seconds and asymptote of 0.17. (B) Collected results for inhibition by 100 nM (32 ± 8%, n = 4), 300 nM (55 ± 2%, n = 5), and 1 μM A-887826 (80 ± 2%, n = 5). Measurements were made after at least 60 seconds of drug exposure in each cell.

As for cloned human channels, A-887826 inhibition of native mouse Nav1.8 channels was relieved by repetitive stimulation at moderate frequencies (Fig. 8A). In control, delivering 5-millisecond steps to +20 mV at 5 Hz produced a small amount of use-dependent reduction, likely reflecting some entry into slow inactivated states that did not recover completely between stimulations (Rush et al., 1998; Blair and Bean, 2003; Tripathi et al., 2006). In the presence of 1 μM A-887826, which reduced the current evoked by slow (0.05 Hz) stimulation to about 20% of control, delivering 5-millisecond depolarizations to +20 mV at 5 Hz produced dramatic relief of inhibition, beginning at the second depolarization and becoming maximal by the 40th or 50th pulse (Fig. 8, B and C).

Relief of Inhibition by Action Potential Waveforms. The relief of inhibition by relatively brief depolarizations raises the question of whether inhibition can be relieved by action potential waveforms. We tested this point by examining inhibition by A-887826 of current evoked by action potential waveforms (Fig. 9). An action potential waveform recorded at 37°C from a small-diameter mouse DRG neuron was used as the voltage command. A-887826 applied at 1 μM greatly reduced the peak TTX-resistant sodium current evoked by the action potential waveform applied at low rates (0.05 Hz), and increasing the stimulation rate to 5 Hz produced substantial relief of inhibition, with peak current evoked by the action potential increasing from 6 ± 2% of control for the first action potential to 30 ± 5% of control for the 100th action potential (n = 5, P = 0.0025, two-tailed paired t test). These data suggest that relief of inhibition by A-887826 can occur during natural firing patterns of nociceptors.

Discussion

These results show that the Nav1.8 inhibitor A-887826 has the unusual property that inhibition is dramatically reduced by repetitive short depolarizations. Such "reverse use dependence" was previously observed for effects of A-803467 (Browne et al., 2009a, b) on human Nav1.8 channels, but the effect is far more prominent for A-887826 than for A-803467. The effect is in striking contrast to other small-molecule inhibitors of Nav1.8 channels, such as lidocaine (Leffler et al., 2007), vinpocetine (Zhou et al., 2003), carbamazepine (Cardenas et al., 2006), tetracaine (Browne et al., 2009a), ambroxol (Leffler et al., 2010), and PF-01247324 (Payne et al., 2015), which all show enhancement of inhibition by repetitive stimulation. The relief of inhibition by repetitive short depolarizations was even more prominent for native Nav1.8 channels in mouse DRG neurons than for human Nav1.8 channels heterologously expressed in CHO cells.

During depolarizing steps, channels convert from resting states to open states and then to inactivated states. In principle, the relief of inhibition could occur if either open states or

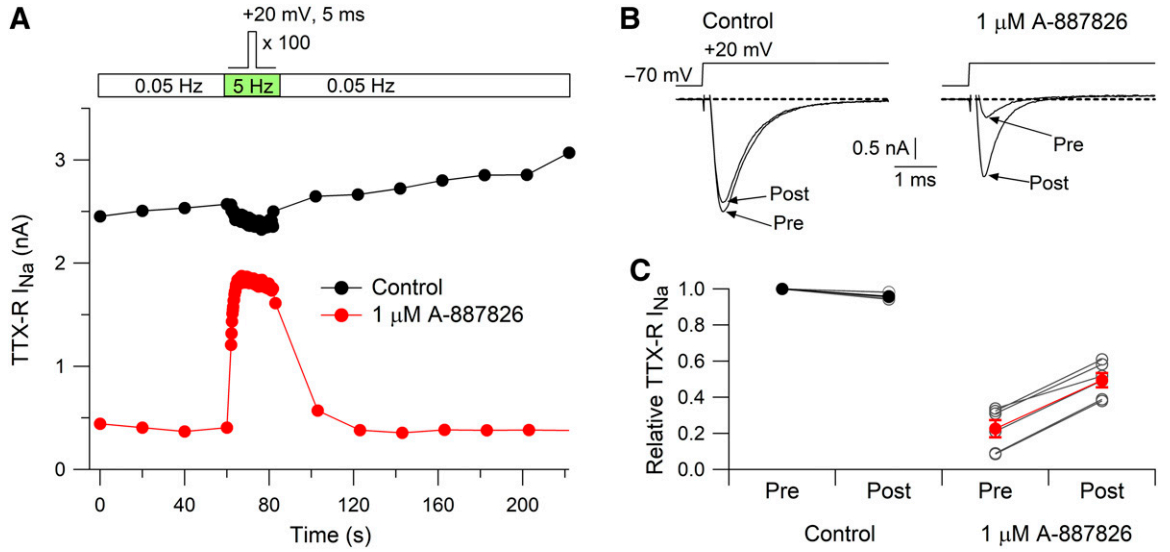

Fig. 8. Use-dependent relief of A-887826 inhibition of mouse TTX-R Na channels. (A) Effect of a train of 100 5-millisecond steps to +20 mV delivered at 5 Hz on peak current in control (black) and after inhibition by 1 μM A-887826 (red). (B) Current evoked by steps from −70 mV to +20 mV before and after the 5 Hz train for the experiment in (A). (C) Collected results for this experimental protocol. Currents in 1 μM A-887826 were normalized by currents evoked at 0.05 Hz in control just before application of A-887826. Open gray symbols: normalized currents before and after the 5 Hz train in individual cells. Closed symbols: mean ± S.E.M. for collected results (n = 6 for both control and 1 μM A-887826).

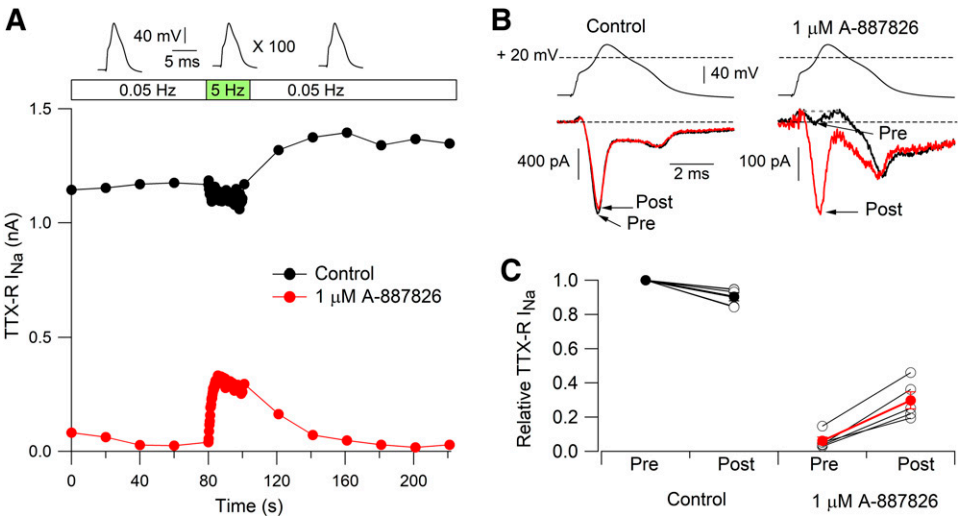

Fig. 9. Inhibition of mouse TTX-R Na current is relieved by action potential waveforms delivered at 5 Hz. (A) Time course of peak TTX-R current evoked by a previously recorded action potential waveform delivered at 0.05 Hz and then (for a 20-second interval) at 5 Hz, first in the absence (black symbols) and then in the presence (red symbols) of 1 μM A-887826. (B) Currents evoked by the first (black) and the last (red) action potential waveforms during the 5-Hz stimulation period in control (left) and 1 μM A-887826 (right). (C) Collected results for change in peak TTX-R current during a 20-second period of stimulation at 5 Hz. Currents in 1 μM A-887826 were normalized to currents evoked at 0.05 Hz before application of A-887826.

inactivated states had reduced affinity for binding the compound. The dependence of relief of inhibition on pulse length suggests that the relief of inhibition is better correlated with the time channels spend in the inactivated state rather than the open state, suggesting that the compound dissociates from inactivated states of the channel. The ability of single 500-millisecond depolarizations to relieve inhibition as effectively as repeated 20-millisecond depolarizations suggests that the compound can dissociate from channels in slow inactivated states as well as from fast inactivated states. When relief of inhibition was produced by single 500-millisecond depolarizations, a striking feature was that the degree of relief was steeply voltage dependent in the range from −10 mV to +40 mV. Entry into slow inactivated states is nearly saturated by about 0 mV, so this voltage dependence is not easily interpreted as identifying either fast inactivated or slow inactivated states as the channel state from which drug unbinding occurs most readily. A-887826 is not a charged molecule, so it is unlikely that the voltage dependence reflects a direct effect of voltage on binding of the molecule in the channel pore. Previous data suggests the existence of multiple slow inactivated states of Nav1.8 channels (Zhang and Bean, 2021), so one possibility is that the voltage dependence of relief by long depolarizations reflects differences in binding affinity to distinct slow inactivated states occupied with different voltage dependence. With cloned hNav1.8 channels, it is also possible that drug unbinding could occur from open channels associated with the component of persistent current present during moderate and long depolarizations. However, the native TTX-resistant current in DRG neurons had very little or no persistent current during steps to +20 mV that produced effective relief of inhibition (Fig. 8B), so at least in these channels, unbinding from inactivated states seems more likely. One possibility is that unbinding of drug could be favored by all states in which the S4 voltage sensors have moved from their internal to external positions, which would include persistent open states when they are present, fast inactivated states, and slow inactivated states.

A recent study used cryo-electron microscopy to show A-803467 bound to Nav1.8 channels at a site within the pore below the selectivity filter (Huang et al., 2022). Whether A-887826 also binds in this region remains uncertain because it is a larger molecule with a significantly different structure (Zhang et al., 2010). The channel structure with A-803467 bound does not immediately suggest why there is use-dependent relief of inhibition, which is quite modest with A-803467 (Browne et al., 2009a, b; Fig. 3, A and C). The biochemical preparation of channels for cryo-electron microscopy is likely to place channels in states corresponding to many minutes or hours at 0 mV, presumably slow inactivated or ultraslow inactivated states. Because Nav1.8 channels apparently enter distinct slow inactivated states as the length of depolarization is increased in the range from 300 milliseconds to 10 seconds (Zhang and Bean, 2021), it is difficult to relate the channel structure resolved in cryo-electron microscopy to the states studied in electrophysiology experiments. Further work will be required to understand the structural basis of the dramatic relief of inhibition of A-887826 by depolarization. A prediction might be that binding is stronger in resting channels than in inactivated channels, but since it has been so far impossible to lock mammalian sodium channels in a resting state in biochemical preparations, this will be challenging to detect in structural experiments.

Although A-887826 is a more potent inhibitor than A-803467 when applied at slow stimulation rates (Zhang et al., 2010; Fig. 1), the use-dependent relief of inhibition is much more prominent with A-887826 than with A-803467. For native Nav1.8 channels, prominent relief of inhibition by A-887826 was evident with action potential waveforms applied at 5 Hz, well within the normal firing rate of nociceptors. This suggests that the effect could act to limit the efficacy of the compound in inhibiting pain signaling in nociceptors, for which conventional use-dependent enhancement of inhibition is very likely advantageous. It will be interesting to see if Nav1.8 inhibitors based on other scaffolds (Payne et al., 2015; Brown et al., 2019; Sun et al., 2019; Tong et al., 2021) also show use-dependent relief of inhibition. If so, it should probably be regarded as a property to avoid in optimizing compounds for pain relief. The substantially weaker degree of use-dependent relief of inhibition by A-803467 compared with A-887826 suggests that it might be possible to phenomenologically establish structure-function relationships for the effect, even if a detailed understanding of how it arises from changes in channel structure during gating will likely be difficult to determine in the near future.

Note Added in Proof: It was discovered the structures were placed incorrectly in Figure 1A when published in the Fast Forward version that appeared online January 12, 2023. Figure 1A has now been corrected.

Authorship Contributions

Participated in research design: Jo, Zhang, Bean.

Conducted experiments: Jo, Zhang.

Performed data analysis: Jo, Zhang, Bean.

Wrote or contributed to the writing of the manuscript: Jo, Zhang, Bean.

References

Bennett DL, Clark AJ, Huang J, Waxman SG, and Dib-Hajj SD (2019) The Role of Voltage-Gated Sodium Channels in Pain Signaling. *Physiol Rev* **99**:1079–1151.

Blair NT and Bean BP (2002) Roles of tetrodotoxin (TTX)-sensitive Na+ current, TTX-resistant Na+ current, and Ca2+ current in the action potentials of nociceptive sensory neurons. *J Neurosci* **22**:10277–10290.

Blair NT and Bean BP (2003) Role of tetrodotoxin-resistant Na+ current slow inactivation in adaptation of action potential firing in small-diameter dorsal root ganglion neurons. *J Neurosci* **23**:10338–10350.

Bosmans F, Puopolo M, Martin-Eauclaire MF, Bean BP, and Swartz KJ (2011) Functional properties and toxin pharmacology of a dorsal root ganglion sodium channel viewed through its voltage sensors. *J Gen Physiol* **138**:59–72.

Brown AD, Bagal SK, Blackwell P, Blakemore DC, Brown B, Bungay PJ, Corless M, Crawforth J, Fengas D, Fenwick DR, et al. (2019) The discovery and optimization of benzimidazoles as selective $Na_V1.8$ blockers for the treatment of pain. *Bioorg Med Chem* **27**:230–239.

Browne LE, Blaney FE, Yusaf SP, Clare JJ, and Wray D (2009a) Structural determinants of drugs acting on the Nav1.8 channel. *J Biol Chem* **284**:10523–10536.

Browne LE, Clare JJ, and Wray D (2009b) Functional and pharmacological properties of human and rat NaV1.8 channels. *Neuropharmacology* **56**:905–914.

Cardenas CA, Cardenas CG, de Armendi AJ, and Scroggs RS (2006) Carbamazepine interacts with a slow inactivation state of NaV1.8-like sodium channels. *Neurosci Lett* **408**:129–134.

Carter BC and Bean BP (2009) Sodium entry during action potentials of mammalian neurons: incomplete inactivation and reduced metabolic efficiency in fast-spiking neurons. *Neuron* **64**:898–909.

Chen WN, Lee CH, Lin SH, Wong CW, Sun WH, Wood JN, and Chen CC (2014) Roles of ASIC3, TRPV1, and NaV1.8 in the transition from acute to chronic pain in a mouse model of fibromyalgia. *Mol Pain* **10**:40.

Choi J-S, Dib-Hajj SD, and Waxman SG (2007) Differential slow inactivation and use-dependent inhibition of Nav1.8 channels contribute to distinct firing properties in IB4+ and IB4- DRG neurons. *J Neurophysiol* **97**:1258–1265.

Cummins TR, Dib-Hajj SD, Black JA, Akopian AN, Wood JN, and Waxman SG (1999) A novel persistent tetrodotoxin-resistant sodium current in SNS-null and wild-type small primary sensory neurons. *J Neurosci* **19**:RC43.

Cummins TR and Rush AM (2007) Voltage-gated sodium channel blockers for the treatment of neuropathic pain. *Expert Rev Neurother* **7**:1597–1612.

Cummins TR, Sheets PL, and Waxman SG (2007) The roles of sodium channels in nociception: Implications for mechanisms of pain. *Pain* **131**:243–257.

Dib-Hajj SD, Binshtok AM, Cummins TR, Jarvis MF, Samad T, and Zimmermann K (2009) Voltage-gated sodium channels in pain states: role in pathophysiology and targets for treatment. *Brain Res Brain Res Rev* **60**:65–83.

Goodwin G and McMahon SB (2021) The physiological function of different voltage-gated sodium channels in pain. *Nat Rev Neurosci* **22**:263–274.

Han C, Huang J, and Waxman SG (2016) Sodium channel Nav1.8: Emerging links to human disease. *Neurology* **86**:473–483.

Hijma HJ, Siebenga PS, de Kam ML, and Groeneveld GJ (2021) A Phase 1, Randomized, Double-Blind, Placebo-Controlled, Crossover Study to Evaluate the Pharmacodynamic Effects of VX-150, a Highly Selective NaV1.8 Inhibitor, in Healthy Male Adults. *Pain Med* **22**:1814–1826.

Huang X, Jin X, Huang G, Huang J, Wu T, Li Z, Chen J, Kong F, Pan X, and Yan N (2022) Structural basis for high-voltage activation and subtype-specific inhibition of human $Na_v1.8$. *Proc Natl Acad Sci USA* **119**:e2208211119.

Jarvis MF, Honore P, Shieh C-C, Chapman M, Joshi S, Zhang X-F, Kort M, Carroll W, Marron B, Atkinson R, et al. (2007) A-803467, a potent and selective Nav1.8 sodium channel blocker, attenuates neuropathic and inflammatory pain in the rat. *Proc Natl Acad Sci USA* **104**:8520–8525.

Jayakar S, Shim J, Jo S, Bean BP, Singeç I, and Woolf CJ (2021) Developing nociceptor-selective treatments for acute and chronic pain. *Sci Transl Med* **13**:eabj9837.

Joshi SK, Honore P, Hernandez G, Schmidt R, Gomtsyan A, Scanio M, Kort M, and Jarvis MF (2009) Additive antinociceptive effects of the selective Nav1.8 blocker A-803467 and selective TRPV1 antagonists in rat inflammatory and neuropathic pain models. *J Pain* **10**:306–315.

Laux-Biehlmann A, Boyken J, Dahllöf H, Schmidt N, Zollner TM, and Nagel J (2016) Dynamic weight bearing as a non-reflexive method for the measurement of abdominal pain in mice. *Eur J Pain* **20**:742–752.

Leffler A, Reiprich A, Mohapatra DP, and Nau C (2007) Use-dependent block by lidocaine but not amitriptyline is more pronounced in tetrodotoxin (TTX)-Resistant Nav1.8 than in TTX-sensitive Na+ channels. *J Pharmacol Exp Ther* **320**:354–364.

Leffler A, Reckzeh J, and Nau C (2010) Block of sensory neuronal Na+ channels by the secreolytic ambroxol is associated with an interaction with local anesthetic binding sites. *Eur J Pharmacol* **630**:19–28.

Liu PW, Blair NT, and Bean BP (2017) Action Potential Broadening in Capsaicin-Sensitive DRG Neurons from Frequency-Dependent Reduction of Kv3 Current. *J Neurosci* **37**:9705–9714.

Obeng S, Hiranita T, León F, McMahon LR, and McCurdy CR (2021) Novel Approaches, Drug Candidates, and Targets in Pain Drug Discovery. *J Med Chem* **64**:6523–6548.

Payne CE, Brown AR, Theile JW, Loucif AJ, Alexandrou AJ, Fuller MD, Mahoney JH, Antonio BM, Gerlach AC, Printzenhoff DM, et al. (2015) A novel selective and orally bioavailable Nav 1.8 channel blocker, PF-01247324, attenuates nociception and sensory neuron excitability. *Br J Pharmacol* **172**:2654–2670.

Rahman W and Dickenson AH (2015) Osteoarthritis-dependent changes in antinociceptive action of Nav1.7 and Nav1.8 sodium channel blockers: An in vivo electrophysiological study in the rat. *Neuroscience* **295**:103–116.

Roy ML and Narahashi T (1992) Differential properties of tetrodotoxin-sensitive and tetrodotoxin-resistant sodium channels in rat dorsal root ganglion neurons. *J Neurosci* **12**:2104–2111.

Rush AM, Bräu ME, Elliott AA, and Elliott JR (1998) Electrophysiological properties of sodium current subtypes in small cells from adult rat dorsal root ganglia. *J Physiol* **511**:771–789.

Sun JF, Xu YJ, Kong XH, Su Y, and Wang ZY (2019) Fenamates inhibit human sodium channel Nav1.7 and Nav1.8. *Neurosci Lett* **696**:67–73.

Tong K, Zhang R, Ren F, Zhang T, He J, Cheng J, Yu Z, Ren F, Zhang Y, and Shi W (2021) Synthesis and Evaluation of Novel α-Aminoamides Containing Benzoheterocyclic Moiety for the Treatment of Pain. *Molecules* **26**:1716.

Tripathi PK, Trujillo L, Cardenas CA, Cardenas CG, de Armendi AJ, and Scroggs RS (2006) Analysis of the variation in use-dependent inactivation of high-threshold tetrodotoxin-resistant sodium currents recorded from rat sensory neurons. *Neuroscience* **143**:923–938.

Urru M, Muzzi M, Coppi E, Ranieri G, Buonvicino D, Camaioni E, Coppini R, Pugliese AM, Tanaka B, Estacion M, et al. (2020) Dexpramipexole blocks Nav1.8 sodium channels and provides analgesia in multiple nociceptive and neuropathic pain models. *Pain* **161**:831–841.

Yekkirala AS, Roberson DP, Bean BP, and Woolf CJ (2017) Breaking barriers to novel analgesic drug development. *Nat Rev Drug Discov* **16**:810.

Zhang HB and Bean BP (2021) Cannabidiol Inhibition of Murine Primary Nociceptors: Tight Binding to Slow Inactivated States of $Na_v1.8$ Channels. *J Neurosci* **41**:6371–6387.

Zhang X-F, Shieh C-C, Chapman ML, Matulenko MA, Hakeem AH, Atkinson RN, Kort ME, Marron BE, Joshi S, Honore P, et al. (2010) A-887826 is a structurally novel, potent and voltage-dependent Na(v)1.8 sodium channel blocker that attenuates neuropathic tactile allodynia in rats. *Neuropharmacology* **59**:201–207.

Zhou X, Dong XW, Crona J, Maguire M, and Priestley T (2003) Vinpocetine is a potent blocker of rat NaV1.8 tetrodotoxin-resistant sodium channels. *J Pharmacol Exp Ther* **306**:498–504.

Address correspondence to: Bruce P. Bean, Department of Neurobiology, Harvard Medical School, 220 Longwood Avenue, Boston, MA 02115. E-mail: bruce_bean@hms.harvard.edu